

Self-Tuning Hamiltonian Monte Carlo for Accelerated Sampling

Henrik Christiansen,^{a)} Federico Errica,^{b)} and Francesco Alesiani^{c)}

NEC Laboratories Europe GmbH, Kurfürsten-Anlage 36, 69115 Heidelberg, Germany.

(Dated: 26 September 2023)

The performance of Hamiltonian Monte Carlo crucially depends on its parameters, in particular the integration timestep and the number of integration steps. We present an adaptive general-purpose framework to automatically tune these parameters based on a loss function which promotes the fast exploration of phase-space. For this, we make use of a fully-differentiable set-up and use backpropagation for optimization. An attention-like loss is defined which allows for the gradient driven learning of the distribution of integration steps. We also highlight the importance of jittering for a smooth loss-surface. Our approach is demonstrated for the one-dimensional harmonic oscillator and alanine dipeptide, a small protein common as a test-case for simulation methods. We find a good correspondence between our loss and the autocorrelation times, resulting in well-tuned parameters for Hamiltonian Monte Carlo.

I. INTRODUCTION

Simulations of biomolecular systems are predominately performed using either molecular dynamics (MD)¹ or (random walk) Monte Carlo (MC)² simulations. While the former method, in its basic formulation, solves Newtons equations numerically, the latter (directly) samples from the target distribution. Both approaches can be used to sample the canonical ensemble, i.e., a system in contact with a thermal bath and can, for many purposes, be used as plug-in replacements for sampling (as long as dynamic properties are not needed). *A priori*, there is thus no apparent advantage of one method over the other.

In MD, time needs to be discretized, and the equation of motions are integrated numerically. This introduces short-time errors as well as accumulating errors, leading for example to a violation of energy conservation (for microcanonical simulations) in the long-time limit.³ While small enough time steps are important for the correct physical evolution (small deviations of the simulated Hamiltonian), they lead to severely impeded dynamics since the system only slowly moves through phase-space. Additional complications are introduced when the system is coupled to a thermostat; there, the velocities as proxy for the system's temperature are modified. There is no canonical way to do this, manifested by many alternative approaches available in the literature.⁴

In MC, on the other hand, there is no error introduced by numerical integration and no adverse effects from controlling the temperature, as this is directly manifested in the acceptance probability. However, one needs to generate trial configurations in a clever way, i.e., to come up with a move set which constitutes major configuration changes without being penalized by a very low acceptance. There are a couple of well accepted move-sets for different systems incorporating prior knowledge which

are based on intuition/heuristic arguments. However, by definition, finding an *optimal* move set is not possible. Traditionally, the proposed moves are random, i.e., their proposal probability does not depend on the current configuration in order to guarantee detailed balance.

In the literature, there already exist a couple of approaches to combine both methods^{3,5}, where one of the most studied one is Hamiltonian Monte Carlo (HMC)⁶⁻⁸, which originally was introduced as hybrid Monte Carlo.⁹ The basic idea is to propagate the system using a (micro-canonical) integrator for a given number of steps which conserves the total energy as used in MD simulations, but add an acceptance of proposals obtained in this way using MC. In case of rejection of a move, the system is reset (in the typical MC fashion) to the previous state. The additional step required for HMC is to randomly draw new velocities, as otherwise the resulting configuration would be identical after rejection. Compared to the individual methods on their own, this combined approach has the advantage that there is no adverse effect of the numerical integration or external control of temperature, while providing a systematic way to propose trial configurations.

The trial configurations proposed by this approach can have a high acceptance probability, especially for small timesteps and few integration steps, as then both the numeric error and the integration error is small (the total energy is in principle conserved by the integrator). Choosing both these parameters small, however, leads again to slow phase space exploration, whereas choosing them large results in the simulation of a shadow Hamiltonian and fast accumulation of numeric errors resulting in small acceptance rates. This implies that there is some balance between those two effects, for which the simulation is much faster at exploring the phase-space.

We will present a fully-differentiable framework which allows to tune both these parameters via backpropagation^{10,11} based on a local loss definition. Further, we will also extend the integrator to include atom-dependent timesteps, which would be very difficult to optimize for using heuristic (gradient uninformed) methods. We investigate two systems: The one-

^{a)}Electronic mail: henrik.christiansen@neclab.eu

^{b)}Electronic mail: federico.errica@neclab.eu

^{c)}Electronic mail: francesco.alesiani@neclab.eu

dimensional harmonic oscillator where we focus on the fundamental mechanisms of the method before turning to demonstrate its performance for the common test system alanine dipeptide.¹² In Section II we give a short overview over the involved simulation methods, followed by a conceptual introduction to the employed fully-differentiable set-up and loss definition in Section III. Section IV presents results for both systems, discussing the achieved improvements in simulation speed and an analysis of the learning process and obtained parameters. Finally, we will conclude and give an outlook about future research in Section V

II. SIMULATION METHODS

In the following, our goal is to simulate a classical system, which consists of particles/atoms interacting via classical potentials. This system is in coupled to a heat-bath, i.e., our target is to simulate in the canonical ensemble. Then, each microstate described by the coordinates \mathbf{x} occurs with a probability that is given by

$$P^{\text{eq}}(\mathbf{x}) = \frac{1}{Z} e^{-U(\mathbf{x})/(kT)}, \quad (1)$$

where $Z = \int e^{-U(\mathbf{x})/kT} d\mathbf{x}$ is the partition function (in statistic often simple referred to as normalizing constant), $U(\mathbf{x})$ is the (potential) energy of a microstate depending on the atoms positions, k is the Boltzmann constant, and T is the temperature of the heatbath. While the evaluation of the partition function would provide access to many thermodynamic observables, this is in practice not possible since this necessitates a summation over all possible microstates. Instead, one attempts to approximate expectation values of quantities of interest at a fixed temperature by producing samples from the target distribution, utilizing methods that do not rely on the value of Z .

A. Monte Carlo

In MC, producing samples from the target distribution is conceptually, *a priori*, straightforward.^{13,14} The main idea behind a Monte Carlo simulation is to build a Markov chain, starting with a random configuration of the system at interest and subsequently progressing by proposing new configurations (which only depend on the current configuration). There is some freedom in choosing the transition probabilities $W_{ij} = W(\xi_i, \xi_j)$ between microstate ξ_i and ξ_j . In MC for molecular systems, typically $\xi = \mathbf{x}$, i.e., a set of Cartesian coordinates, but in general this can be any configurational information. One of the most flexible choices for the acceptance criterion between states is the original Metropolis algorithm¹⁵ which reads

$$w_{ij} = w(\xi_i, \xi_j) = \min \left(1, \frac{f(\xi_j, \xi_i) P^{\text{eq}}(\xi_j)}{f(\xi_i, \xi_j) P^{\text{eq}}(\xi_i)} \right), \quad (2)$$

where $f_{ij} = f(\xi_i, \xi_j)$ is the proposal probability for a potential update to a new microstate. Here, the partition function cancels, since one is only interested in the ratio of the equilibrium distributions. This then leads to the transition probability

$$W_{ij} = \begin{cases} f_{ij} w_{ij} & j \neq i \\ f_{ii} + \sum_{j \neq i} f_{ij} (1 - w_{ij}) & j = i \end{cases}. \quad (3)$$

Using this prescription, it is easy to see that the detailed balance condition given by

$$W_{ij} P_i^{\text{eq}} = W_{ji} P_j^{\text{eq}} \quad (4)$$

is fulfilled. This is a sufficient condition for the convergence to the equilibrium distribution. In many practical implementations the proposal probability is often chosen to be independent of the configuration, i.e., $f_{ij} = f_{ji}$. If the proposals are not symmetric, this acceptance is often referred to as Metropolis-Hastings criterion.¹⁶ There are many ways to propose configurational changes to the system, which then constitute the move set. The “optimal” set depends highly on the system and its parameters. Typically, for polymeric systems, local updates of atom positions are complemented by large conformational changes such as pivot moves at higher temperatures, and bond-rebridging moves at low temperature.¹⁷ States first represent the equilibrium distribution after an initial relaxation/burn-in period. Indeed, while often discarded, this initial period is also of great interest, allowing for the study of many nonequilibrium processes^{18,19}, which even facilitate the extraction of equilibrium exponents in some cases.^{20,21}

B. Molecular Dynamics

While in MC of a classical system one is only concerned with the (potential) energy of the system given by the particles positions \mathbf{x} , in MD one simulates the combined distribution of coordinates and velocities \mathbf{v} , i.e., one has $\xi = (\mathbf{x}, \mathbf{v})$. Further, in standard MD, one simulates in the microcanonical ensemble, manifesting in conserved total energy $H(\xi) = H(\mathbf{x}, \mathbf{v}) = U(\mathbf{x}) + K(\mathbf{v})$, where the potential energy $U(\mathbf{x})$ depends only on the coordinates \mathbf{x} and the kinetic energy $K(\mathbf{v})$ depending on the momenta \mathbf{v} . This is achieved by iteratively integrating the equation of motions, where the most common prescription used is the velocity Verlet algorithm²², consisting of the following steps

$$\mathbf{v}_i \left(t + \frac{1}{2} \Delta t_i \right) = \mathbf{v}_i(t) + \frac{1}{2} \mathbf{a}_i(t) \Delta t_i \quad (5a)$$

$$\mathbf{x}_i(t + \Delta t_i) = \mathbf{x}_i(t) + \mathbf{v}_i \left(t + \frac{1}{2} \Delta t_i \right) \Delta t_i \quad (5b)$$

$$\text{Recalculate } \mathbf{a}_i(t + \Delta t_i) \text{ from the new positions} \quad (5c)$$

$$\mathbf{v}_i(t + \Delta t_i) = \mathbf{v}_i \left(t + \frac{1}{2} \Delta t_i \right) + \frac{1}{2} \mathbf{a}_i(t + \Delta t_i) \Delta t_i \quad (5d)$$

where i is the index of the atom, Δt_i is the (atom dependent) timestep, and $\mathbf{a}_i = -m^{-1}\partial/\partial\mathbf{x}_i U(\mathbf{x})$ is the acceleration acting on the atom obtained from the potential. This integrating step is performed iteratively, until enough statistics is gathered to estimate the desired properties. In a standard MD simulation, the individual atoms need to evolve synchronously in time, which practically restricts the use of timestep to a global definition of $\Delta t_i = \Delta t$, i.e., the timestep is not dependent on the atom index. That also implies that the maximal timestep which can be used is determined by the fastest mode of oscillation.

To sample from P^{eq} in the canonical ensemble using MD, one has to additionally find a method to control the velocities, for which there is no natural way.⁴ That means, there are many ways to achieve this, which have certain advantages and disadvantages. In the canonical ensemble for MD, one reproduces the Boltzmann distribution of the total energy

$$P^{\text{eq}}(\boldsymbol{\xi}) = P^{\text{eq}}(\mathbf{x}, \mathbf{v}) = \frac{e^{-H(\mathbf{x}, \mathbf{v})/kT}}{\int e^{-U(\mathbf{x})/kT} d\mathbf{x} \int e^{-K(\mathbf{v})/kT} d\mathbf{v}}, \quad (6)$$

which factorizes into the canonical distribution of the potential energy and of the momenta

$$P^{\text{eq}}(\mathbf{x}, \mathbf{v}) = \frac{e^{-U(\mathbf{x})/kT}}{\int e^{-U(\mathbf{x})/kT} d\mathbf{x}} \frac{e^{-K(\mathbf{v})/kT}}{\int e^{-K(\mathbf{v})/kT} d\mathbf{v}} \quad (7)$$

$$= P^{\text{eq}}(\mathbf{x}) P^{\text{eq}}(\mathbf{v}).$$

Not all thermostats produce the canonical ensemble, so special care has to be taken to make the right choice.⁴ Especially, some thermostats are only canonical in $P^{\text{eq}}(\mathbf{x})$, but not in the joint distribution $P^{\text{eq}}(\mathbf{x}, \mathbf{v})$.

We also want to highlight that sampling using MD is only approximate, i.e., the convergence to the target distribution is only guaranteed in the limit of $\Delta t \rightarrow 0$. In contrast, MC sampling is asymptotically exact.

C. Hamiltonian Monte Carlo

HMC combines elements from MD and MC: Microcanonical MD simulations are used as proposals for the MC accept/reject step. This combination of methods was originally proposed by Duane et al.⁹ and later popularized in the statistics community with applications towards inference of Bayesian neural networks.⁶ While recent work exists highlighting the performance of HMC²³, and it is implemented in or for commonly used simulation packages^{24–26}, it is often not the go-to method of choice. In part, this is probably due to the belief that this method becomes ineffective for simulations of large and complex systems, although recent work suggests otherwise.²³ Another part lacking in its acceptance is the problem of choosing optimal parameters of the simulation, as will become clear in the following.

For this method, we again have both particle positions and velocities as our state, i.e., $\boldsymbol{\xi} = (\mathbf{x}, \mathbf{v})$. While the

interpretation of having a velocity is quite natural from a physical point of view, it is not as straight forward in many other fields of applications, for which one talks about extending the phase-space. Indeed, also in the physics literature one finds instances where it is not clear how to define the velocities.²⁷ The steps of HMC are as follows:

1. Draw velocities \mathbf{v}_i according to Maxwell-Boltzmann distribution, generating the initial state $\boldsymbol{\xi}_i = (\mathbf{x}_i, \mathbf{v}_i)$. This sets a new level of total energy $H(\boldsymbol{\xi}_i)$.
2. Propagate the system according to Eqs. (5) for n steps with fixed Δt_i , resulting in our proposal configuration $\boldsymbol{\xi}_j$. The integration steps are performed in the microcanonical ensemble, corresponding to in principle conserved total energy H (in practice, this is of course not the case due to the discretization in time).
3. The new state $\boldsymbol{\xi}_j$ is then accepted according to Eq. (2). If the proposal is rejected, the system is reset to $\mathbf{x} = \mathbf{x}_i$ and one continues at step 1.

There are some important details of this procedure which we will discuss in the following. In practice, it is beneficial to not use constant Δt_i but to rather pick from a distribution. This is referred to as jittering⁶ and avoids some problems related to repeatedly running into small unfavorable regions in phase-space due to the deterministic dynamics.⁶ In our simulations, we pick the timesteps from a normal distribution with fixed relative variance, i.e.,

$$\Delta t'_i \sim \mathcal{N}(\Delta t_i, s\Delta t_i), \quad (8)$$

where s is a free parameter. We will show the influence and associated problems of not jittering the timestep in the results section, i.e., section IV.

Since the microcanonical integration from $\boldsymbol{\xi}_i$ to $\boldsymbol{\xi}_j$ is deterministic, invertible, and volume-preserving one can simply use the ratio of the target distributions P^{eq} in Eq. 2 since this implies that the proposal probability f_{ij} exactly cancel.^{28,29}

In principle, to make the whole update reversible (necessary to fulfill detailed balance), one would need to invert the velocities \mathbf{v} before performing step 3, but in practice the kinetic energy is invariant to inversion of velocities and new velocities are drawn anyway in step 1.⁶ This also eliminates the need to explicitly implement the forward and backward integration otherwise needed for detailed balance, as the velocities are picked randomly either way. The overall prescription produces a canonical distribution of the total energy, which following Eq. (2) produces our target distribution of Eq. (1).

HMC replaces (or actually can augment) the hand-crafted move sets used in a standard MC simulation. The advantage of this approach is the additional use of the gradient information, which allows for informed moves

that either dissipate or absorb kinetic energy. This way, the acceptance probability is drastically improved while maintaining relatively large conformational changes. In fact, apart from numerical error introduced in the integration, these proposed updates have an acceptance probability close to 100%, since the total energy is conserved. For an effective exploration of phase space, one, however, needs to balance phase space movement and acceptance rates. Indeed, it has been shown in Ref. 30 that the optimal acceptance probability should approach $\alpha = 0.651$ for (vanilla) HMC (under some assumptions using the standard leapfrog integrator), independent of the particular (high dimensional) target. In practice, however, it is not clear if all assumptions hold and it has been found to sometimes perform poorly, especially due to the observation that samplers with the same acceptance rate can exhibit vastly different behavior.³¹

The practical solution often employed is to prescribe a target acceptance rate of around 50% to 60% and heuristically optimize the timestep Δt to take such a value that this is observed on average. A common method to set a good number of integration steps n is called NUTS³², which uses a recursive algorithm to build a set of candidate configurations on the fly. This procedure stops once the so-called U-Turn condition is satisfied, which signifies a doubling back of the trajectory. While this approach works well in practice, in order to preserve detailed balance, there is a need to both consider moves in forward and backward direction which recursively build a tree of steps, from which one then samples the proposal. This can incur a two-fold overhead in performed updates. In Ref. 33 an approach to tune HMC is proposed: The target acceptance probability was combined with an optimization objective based on multiple chains which is able to tune the total trajectory length $n\Delta t$, i.e., to some extent to tune both crucial parameters of HMC. There, it is shown that such an approach can outperform NUTS and finds the optimal parameters one otherwise would only find using a grid search.

Another direction of research is a reparametrization of the simulation space on which HMC is performed, as e.g. proposed in Riemannian HMC³⁴ or via a mapping given by learned functions.^{35–38} While these approaches are promising, at least the former appears to suffer from problems when numerically integrating requiring for example hand-tuning of many parameters.³⁹ A concern for the latter is that the map needs to adequately capture the geometry of the target distribution, as otherwise one would get slow mixing in the tails.³⁷ These methods still require the setting of Δt and n (or possibly more parameters if we choose a more parameterized version of the integrator), i.e., our approach is still applicable in this setting.

We want to note here that the propagation of the system can be performed by any arbitrary function and does not need to follow the structure set in Eqs. (5), i.e., proposals do not need to use the velocity Verlet integrator. One example for this is classical random-walk Monte

Carlo, where changes to the system are typically performed by picking them from a (configuration independent) distribution. For this approach, it is also possible to learn parameters based on gradient information.⁴⁰

Writing the proposal as an arbitrary function of ξ_i instead of using the physically integrator, i.e., using $\xi'_i = g(\xi_i)$, the connection to Normalizing flows becomes clear.^{41–43} In this setting, the determinant of the Jacobian matrix acts as scaling factor between the phase-space volumes (see the standard formula for the change of variables used, e.g., in multidimensional integration), i.e., Eq. (2) reads

$$w_{ij} = \min \left(1, \frac{P^{\text{eq}}(\xi_j)}{P^{\text{eq}}(\xi_i)} \left| \det \left(\frac{\partial g(\xi_i)}{\partial \xi_i} \right) \right| \right). \quad (9)$$

Thus, the general requirement on $g(\xi_i)$ is that we can efficiently calculate the determinant of the Jacobian of the transformation. In practice, one can stack several functions together, forming again a sequence of function calls. This is indeed what the velocity Verlet integrator does, although in such a form that the determinant of the Jacobian is one and does not need to be considered. Changing the timestep or the number of integration steps does not result in a volume changing transformation.

Normalizing flows share the requirement that calculating the determinant of the Jacobian is fast. They are usually used in a somewhat different context and focus on proposing global updates to accelerate sampling, where they are trained to minimize some variant of the Kullback-Leibler divergence for a given target distribution.^{43–45} In this work, we will not consider reparametrizations of the velocity Verlet integrator²² which change phase-volume (such as introduced in Ref. 46), but consider this as an interesting outlook.

III. FULLY DIFFERENTIABLE FRAMEWORK AND OPTIMIZATION OBJECTIVE

Our primary goal is to find good average parameters of the velocity Verlet integrator presented in Eqs. (5), in particular the timesteps Δt_i and the number of integration steps n . Since the number of atoms can grow quite large, this constitutes many correlated parameters that cannot efficiently be optimized for using heuristic methods. This makes the use of a fully differentiable framework very appealing, since then we can use gradient information to update all parameters. Although these optimizers, by definition, only use local information and can be trapped in a local minimum, experience has shown that they are still able to very efficiently find suitable values for the parameters, especially in the context of neural networks.

1. Simulation Set-Up

We achieve a fully differentiable simulation set-up by implementing our algorithm in pyTorch⁴⁷, a software library often used in machine learning. The appeal of this approach is automatic differentiation^{48,49} which allows for the evaluation of partial derivatives of a function specified by a computer program. In pyTorch, any operation applied to the so-called tensors is recorded, so that via the chain rule one is able to calculate the gradient on any parameter of the computation graph. To make changes based on this gradient information, we then need a way to judge the goodness of the output of the computation, i.e., a loss L associated with the integration.

The parameters are then updated depending on the loss using backpropagation^{10,11}, i.e., the derivative of the loss with respect to every parameter θ_i of the computation graph we want to tune is calculated and then used to calculate the change of the parameter

$$\theta'_i = \theta_i - \eta \frac{\partial L}{\partial \theta_i}, \quad (10)$$

where η is the so-called learning rate and θ_i is for example the timesteps Δt_i or the number of integrations steps n . This type of update rule is also called gradient descent, i.e., the parameters are changed in opposite direction of the gradient. Variants of this optimization algorithm exist, which for example also include a momentum variable to accelerate convergence. We will use one of the most popular optimizers incorporating such additional terms, i.e., the Adam optimizer.⁵⁰

2. Autocorrelation and Objective Function

The most common way to evaluate the performance of an MC simulation is to investigate the autocorrelation between subsequent states of the chain. For this, we first recall the definition of the autocorrelation function¹⁴

$$A_{\mathcal{O}}(k) = \frac{\langle \mathcal{O}_i \mathcal{O}_{i+k} \rangle - \langle \mathcal{O}_i \rangle \langle \mathcal{O}_i \rangle}{\langle \mathcal{O}_i^2 \rangle - \langle \mathcal{O}_i \rangle \langle \mathcal{O}_i \rangle}, \quad (11)$$

where $\langle \dots \rangle$ symbolizes the thermodynamic expectation value in equilibrium (after equilibration) when sampling P^{eq} . From the autocorrelation function, one way to obtain the autocorrelation time is

$$\tau_{\mathcal{O}} = \frac{1}{2} + \sum_{k=1}^N A(k) \left(1 - \frac{k}{N}\right). \quad (12)$$

Here, \mathcal{O} is any observable of the system, for example the potential energy which we will use in the following (this implies a different autocorrelation time per observable). The autocorrelation time is related to the effective sample size (ESS)

$$N_{\mathcal{O},\text{eff}} = \frac{N}{2\tau_{\mathcal{O}}}. \quad (13)$$

In practice, we calculate the ESS as implemented in tensorflow⁵¹ where the sum in Eq. (12) is truncated as proposed in Ref. 52. We then use the ESS to estimate the autocorrelation time τ via above relation.

The importance of the autocorrelation time lies in the need to be included when calculating the standard deviation on observables as

$$\sigma_{\mathcal{O}}^2 = \frac{\sigma_{\mathcal{O}}^2}{N_{\mathcal{O},\text{eff}}} = \frac{\sigma_{\mathcal{O}}^2}{N} 2\tau_{\mathcal{O}}. \quad (14)$$

That is, when an algorithm has a smaller autocorrelation time one needs to simulate shorter to achieve the same error on the observable.

However, quantities related to the autocorrelation function cannot be effectively used as an objective for the fully-differentiable set-up since they require long chains to provide reliable estimated of $\tau_{\mathcal{O}}$. Therefore, we make use of a proxy loss to the autocorrelation time, define as

$$L_n = -p_n |\mathbf{x}'_n - \mathbf{x}_0|^b \quad (15)$$

where p_n is the acceptance probability of the proposal and $|\mathbf{x}'_n - \mathbf{x}_0|^b$ is the movement in coordinate phase-space (distance between the start and end states), computed after performing n integration steps, i.e., for each proposal we generate. A common choice is $b = 2$,^{53,54} where one is thus optimizing for the expected squared jump-distance. This definition, however, is not unique and not guaranteed to provide the best correspondence to a reduction in autocorrelation times. For example, an optimal jump in real coordinates does not need to lead to an optimal autocorrelation time for other observables such as the potential energy. Further, the expected jump distance only optimizes for the lag-1 autocorrelation, whereas further values are ignored. It is not clear how well the information about correlations at small lags correlates with the overall shape of the autocorrelation function. This means that there is still some freedom in optimizing the loss function. For example in Ref. 46 the authors introduced an additional reciprocal term which penalized small jumps more strongly and in Refs. 33 and 55 alternative definition relying on multiple chains are proposed, either by evaluating the change in the estimators of the expected squared jump³³ or focusing on difficult directions.⁵⁵ As we will show later, in our case we found that simply setting $b > 2$ provides a better correspondence with the autocorrelation times we observe for the potential energy.

Since our goal is to propagate the system as efficiently as possible in terms of computational effort, the definition of the loss in Eq. (15) is only sufficient when the number of integration steps n is fixed. For our purposes, we introduce a rescaling of the loss by the computational effort, i.e., we define the loss as L_n/n and by this incorporate the information that every integration step takes roughly the same computational effort. Previously, it was empirically found that defining L/\sqrt{n} provides a well working approach in practice³¹, although it is not clear to us why the cost should not enter linearly.

When trying to optimize for n one needs to find a way to include the number of steps n into the computation graph which allows calculating partial derivatives with respect to it and gives a signal for good values. Thus, to learn the optimal (distribution of the) number of integration steps n , we propose to weight the output of every integration step with a learned distribution. For this, we define the loss as

$$L = \sum_{n=1}^N c_n L_n / n, \quad (16)$$

where c_n are the weights of the particular number of integration steps and N is the maximal number of integration steps considered during training. The c_n are in practice obtained as softmax of unrestricted parameters C_n , i.e.,

$$c_n = \sigma(C_n) = \frac{e^{C_n}}{\sum_{n=1}^N e^{C_n}}, \quad (17)$$

where the temperature of the softmax is set to unity. We initialize C_n as uniform random number from zero to one and apply the softmax to arrive at our initial c_n . This approach is inspired by an attention-like set-up⁵⁶ and allows to give “attention” towards a particular integration step. While this approach makes it necessary to set a maximum number of integration steps N during training and always simulate until the maximum is reached, after learning one categorically picks from the probabilities and there is thus no unnecessary computing. While our approach provides a fixed distribution over the steps n , e.g., NUTS³² gives a good number of steps which depend on the particular trajectory. However, some integrations steps can be wasted since in order to preserve detailed balance both forward and backward steps need to be executed, so this trade off may be beneficial nonetheless, as already shown in Ref. 33. The picking from c_n can also serve as a jittering on the number of integration steps and thus helps to avoid problems like local minima in the loss-surface, see our discussion on jittering for Δt in Section II C.

In practice, we also normalize the loss by the number of atoms (usually fixed during a simulation) and the number of epochs in order to arrive at optimal learning rates that are as independent of the system as possible. Since they are only constant factors during training, these do, however, have no influence on the system apart from rescaling the learning rate.

Finally, for molecular systems, there are some further demands towards the loss: Translations and rotations lead, in the naive definition of Eq. (15) to a major decrease in L , whereas in reality the physics of the system has not changed. To circumvent this, there are two possible adaptations: Either we only learn parameters of the integrator which do not (directly) lead to translations (such as Δt_i or n) or one restricts the loss to optimize for translational invariant objectives (such as using the jump in relative distances). In this work, we will follow the first approach.

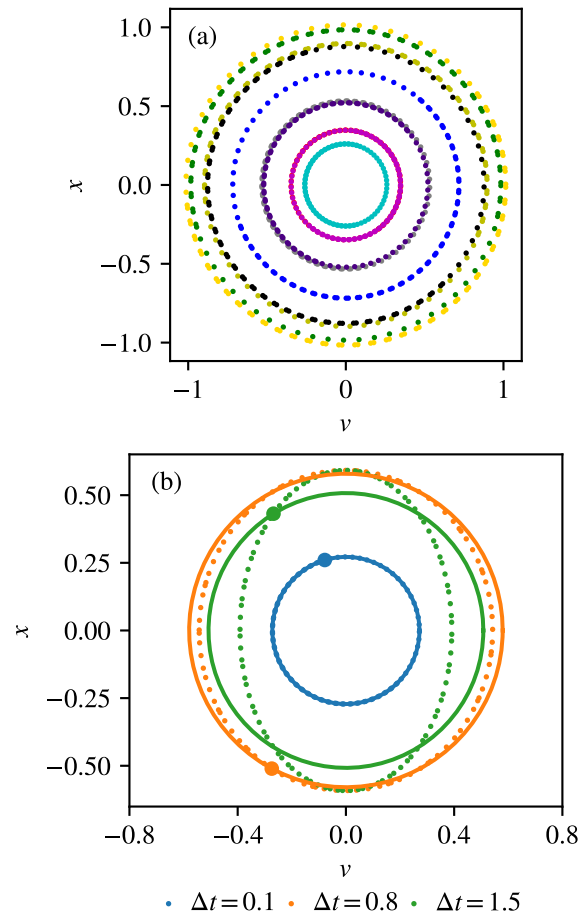


FIG. 1. (a) Example trajectories for x and v of the one-dimensional harmonic oscillator for $\Delta t = 0.1$ at $T = 0.5$ as obtained from HMC with $n = 100$. (b) Influence of the choice of Δt on the simulated (shadow) Hamiltonian using otherwise the same parameters as in (a). The solid lines in the same color as the data points correspond to the analytically expected trajectories. The big dots symbolize the starting point of the trajectory, which sets the expected energy level.

IV. RESULTS

We first validate our approach for a simple test-system in subsection A, the one dimensional harmonic oscillator, which allows us to study the effects of HMC in more detail and visualize some open points of the HMC approach. Following this, we study a physically more realistic system, alanine dipeptide, in section B.

A. Harmonic Oscillator

We start our analysis by considering one of the simplest physical systems: The one-dimensional harmonic oscillator, which can have physical interpretation for example as a pendulum or a spring fixed at the origin at one end with a single mass attached at the other. Our

goal is to understand basic principles of HMC and be able to visualize what is happening for this system. The full Hamiltonian of the harmonic oscillator with mass $m = 1$ and spring constant $k = 1$ is defined as

$$\mathcal{H} = U(x) + K(v) = 0.5(x^2 + v^2), \quad (18)$$

where x is the position and v is the velocity of the mass. Our goal for this exemplary system is to simulate it at a fixed temperature in the canonical ensemble, for which we choose $T = 0.5$ here. We first follow the general recipe of HMC presented in subsection II C.

1. Phase Space and Simulated Shadow Hamiltonian

In Fig. 1(a) we visualize a few sample trajectories of the harmonic oscillator for $\Delta t = 0.1$ and $n = 100$ integration steps obtained from HMC. The trajectories form (near perfect) circles, where the radius is given by energy conservation of the Hamiltonian (18). The different radii of the circles can be understood since at every new iteration the velocity is picked from the Maxwell-Boltzmann distribution, setting a different level of the total energy. With these parameters, the total energy is nearly perfectly conserved, leading to acceptance rates close to 100%. It is well known that it is not ideal to have such high acceptance rates, since phase space can be much more effectively be explored when using a larger Δt , see II C for a more detailed discussion. In principle, increasing Δt for fixed number of integration steps n only changes how fast the phase-space is sampled/explored, i.e., how fast the “circle” is examined. There are, however, a couple of interesting effects: It is well known in the literature, that when using a finite timestep, one only simulates the so-called shadow Hamiltonian^{6,57–59} and not the true Hamiltonian. The difference between these two Hamiltonians can readily be observed for the harmonic oscillator, for which we plot example trajectories (obtained using the velocity Verlet integrator defined in Eqs.(5)) for different Δt in Fig. 1(b) as would be used to obtain a single HMC proposal. While for $\Delta t = 0.1$, the obtained trajectory plotted as dots is (nearly) forming a perfect circle at least on the scale shown here, for $\Delta t = 0.8$ and 1.5 fs the trajectory clearly forms an ellipse with eccentricity $e > 0$. As solid lines in the same color as the data points, we have also drawn the trajectories which should theoretically have been simulated, simply following the energy conservation prescribed by the Hamiltonian (18). These true trajectories start from the initial point of the trajectory marked by the big dot in the same color. It can be clearly seen that the points deviate more from the true circle for increasing Δt . Whenever one observes points on the inside of the circle, this corresponds to a lower total energy and thus acceptance of 100%, whereas points outside the circle have larger total energy and are not always accepted. While one would naively expect that these effects should cancel out since one often starts from a new position, resulting in an average acceptance

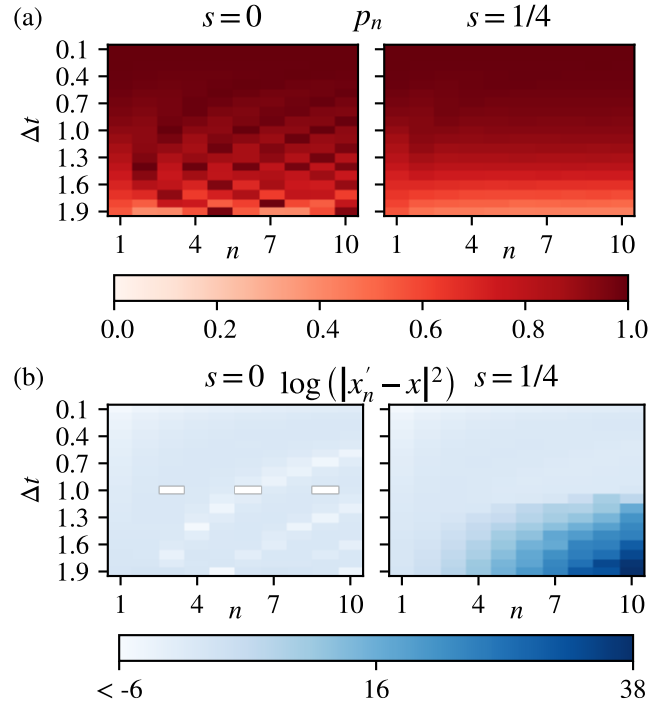


FIG. 2. (a) Acceptance p and (b) logarithm of squared jump $(x'_n - x)^2$ as a function of timestep Δt and number of integration steps n for the one-dimensional harmonic oscillator at $T = 0.5$. Shown are in both cases the results for the not jittered ($s = 0$) and jittered ($s = 1/4$) timestep Δt .

rate in the course of a full HMC simulation, this is not the case. Since the first point of the phase-space sets the initial energy level (which in turn sets the circle) and one always moves along the trajectory the same distance (given by $n\Delta t$) in either forward or backward direction, one sees a periodic behavior of the acceptance rate given by the “deviation from the circle” in Fig. 1.

2. Influence of Jittering

In this section, we will investigate the advantage of jittering the timestep Δt on the dynamics of the harmonic oscillator as an approach to avoid recurring patterns in the simulation. Figure 2(a) shows a heatmap of the acceptance rate p_n as a function of timestep Δt and number of integration steps n for the harmonic oscillator, measured after the system is equilibrated. Without jittering of the timestep Δt , i.e., by setting $s = 0$ in Eq. (8) one observes several minima/maxima in the surface plot, corresponding to small/large acceptance rates. They follow a pattern, which can exactly be explained by the deviations from the true trajectories discussed in Fig. 1(b). When introducing jittering on the timestep, as shown in the same plot where we have used $s = 1/4$, these minima/maxima vanish and one observes as a function of Δt a smooth decay of the acceptance rate p_n . This trend

is also there in the non-jittered simulation, but less visible due to the overlay with the many minima/maxima. This highlights the problem of using a simple criterion of fixed target acceptance rate, as often done when tuning the parameters of HMC. Without jittering, one would pick, depending on the starting parameters, any pair of Δt and n having the desired value of acceptance rate, which does not need to correspond to a small autocorrelation time. For the jittered simulations, one would pick a fixed Δt as local minima/maxima are smoothed out, but without any ability to distinguish between the influence of n on the performance. As we will see later, this does not correlate well with the autocorrelation times of the potential energy.

A similar behavior of multiple local minima/maxima can also be observed for the squared jump distance, which is presented in Fig. 2(b). Here, we have opted to plot it logarithmically, since the differences in the jump are quite large for some parameter configurations. Without jittering ($s = 0$), one observes several minima/maxima in the surface plot, whereas with jittering $s = 1/4$ this is not seen. With jittering, however, finds that the squared jump distance can become huge for the larger Δt and n region, which can be explained by the occasional “breaking” of simulations at large Δt where self-enforcing effects lead to explosions of the values of the position and velocity. This is a well known effect when choosing very large time steps and are typically rejected by the Metropolis-Hastings criterion due to a very large potential energy.

3. Loss Surface

Figure 3(a) and (b) show the loss L_n of Eq. (15) recorded during the HMC run (*without learning*, i.e., only showing the obtained values for the optimization target). The general observation of multiple minima/maxima for the separate acceptance rate and squared jump distance in Fig. 2(a) and (b) also carries over to the loss (correlated expectation value of both) without jitter, see Fig. 3(a). With jitter, as shown in Fig. 3(b), the loss loses this property, and one (clear) global minimum emerges at $\Delta t \approx 1.3$ and $n \approx 2$. Our goal is that the loss serves as a local proxy for the autocorrelation times of our observables, where we here focus on the correlations of the potential energy as a placeholder for many interesting properties of the system. While not optimally, the loss agrees generally well with the (logarithms of the) autocorrelation times for the potential energy presented in Fig. 3(c). The region with lower loss appears to be shifted relatively towards higher Δt , which however is not as detrimental as smaller Δt . Finally, we are, however, interested in the performance per computing effort. For this, we plot L_n/n in Fig. 3(d), which shifts the minimum towards smaller n . The global optimum for this system at $T = 0.5$ is somewhere around $\Delta t \approx 1.75$ and $n \approx 1$. This is also reconfirmed for the autocorrelation time $n\tau$, measured in terms of the computational effort. Here, we also observe that the minima

shift towards smaller n , although not as strongly as for the loss. This is due to the relative difference in the amplitude between minimum/maximum for the loss and autocorrelation time.

4. Learning of HMC Parameters

After having established a good correlation between the loss and the autocorrelation time of the potential energy for this system, we now turn to learning the optimal parameters via the fully differentiable framework, implemented in pyTorch.⁴⁷ We make use of the Adam optimizer⁵⁰ with learning rate $\epsilon = 0.01$ with otherwise default parameters from pyTorch. Before performing on optimization step of Δt and n , we perform 10 proposals in order to average out the resulting gradients, setting our epoch length. The system is initialized for different $\Delta_0 t$ and our attention weights C_n are picked uniformly from zero to one (this means our mean value of the number of steps n is initially $\approx N/2$ and allows for “information” from all integration steps).

In Fig. 4(a) we again show the loss surface of L_n/n presented in Fig. 3(d), but now include sample learning-trajectories for different initial values of $\Delta_0 t$ with the C_n randomly initialized as discussed before. We plot the mean values of the timestep and number of integration steps, i.e., Δt and $\bar{n} = \sum_{i=1}^N n c_n$. It is evident from the visualization of the trajectories that, independent of initial parameter, all curves move towards the region with smaller loss values. This is reinforced by the recorded loss values during training, which we plot as a function of training epoch in Fig. 4(b). Since the data for the recorded loss is very noisy due to the small batch size and few degrees of freedoms of the system leading to little self-averaging, we have calculated a running average over 300 epochs to visualize the training. Especially for $\Delta_0 t = 0.1$ some jumps in the loss are visible, mainly around $t = 3000$. This corresponds to the “jump” from a big weight at $n = 3$ to $n = 2$, which can also be appreciated from Fig. 4(c), where we show the attention weights c_n for different epochs. Initially, at $t = 0$, the weights are nearly uniform, where than for early times at $t = 200$ a small peak forms around $n = 5$. As time progresses, there is a large weight on $n = 3$ which then in the timesteppan from $t \approx 1000$ shifts towards $n = 2$ at $t \approx 3400$. At the final training epoch, the weight is completely on $n = 2$. These observations are consistent with what we see in Fig. 4(a) as movements on the loss surface for $\Delta_0 t = 0.1$.

Having a good correspondence between loss and the autocorrelation of the potential energy allows us to effectively learn good parameters of HMC for this system via the fully differential framework. Next, we will consider a bigger molecular system with more intricate interactions.

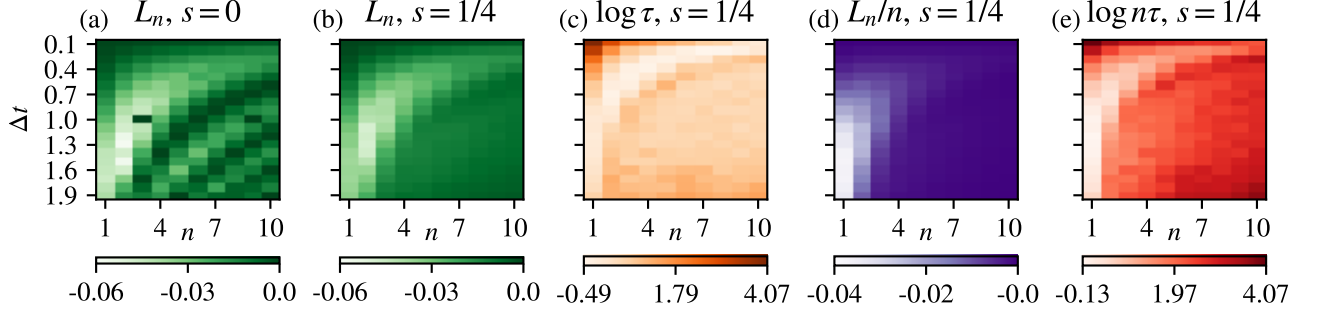


FIG. 3. (a) and (b) show the loss L_N as a function of Δt and n for (a) no jittering ($s = 0$) and (b) with jittering ($s = 1/4$). In (c), we plot the logarithm of the autocorrelation time extracted from the timeseries of the potential energy. The region of desired small autocorrelation times correspond reasonably well to the region where the loss is minimized, as shown in (b). (d) shows the same data as in (b), but the loss is rescaled with the computational effort L_n/n . Finally, in (e) we again show the logarithm of the autocorrelation time, but in units of the computational effort $n\tau$. The logarithm is chosen for the autocorrelation time to highlight the differences, as these are much larger than in the other plots for the losses.

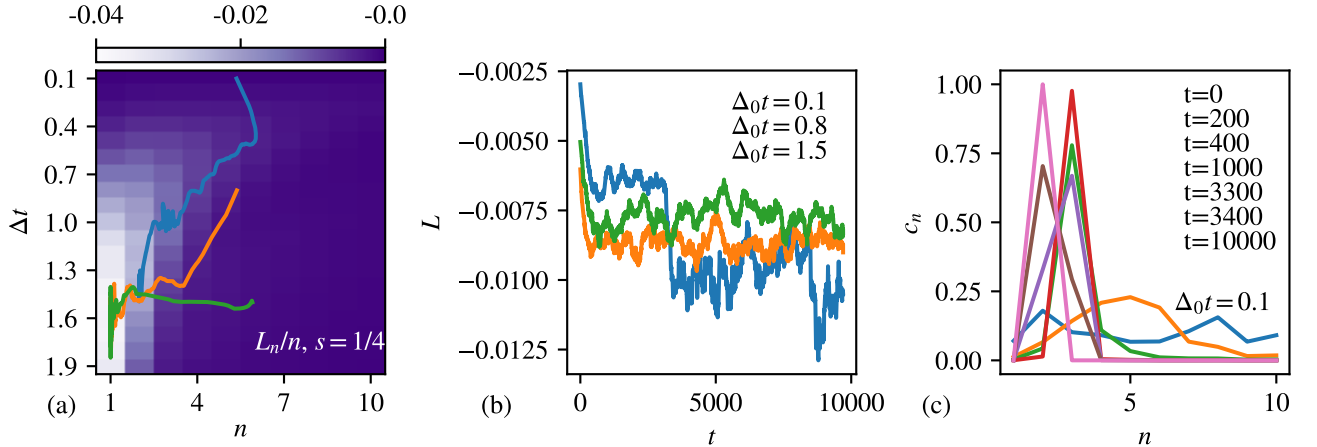


FIG. 4. (a) Loss surface as a function of Δt and n . On top, three example trajectories showing the expectations values of Δt and n during learning for three initial values of the timestep $\Delta_0 t$. (b) The corresponding loss as a function of epochs t for the curves shown in (a). (c) Attention weights c_n for $\Delta_0 t = 0.1$ for different epochs indicated in the legend.

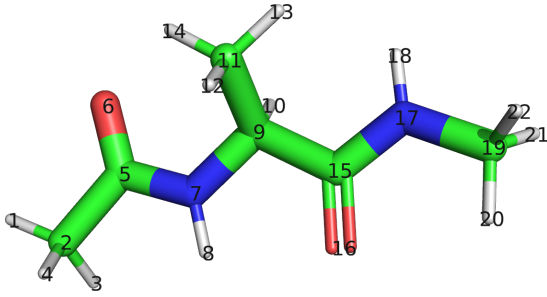


FIG. 5. Graphical representation of alanine dipeptide, where the atoms are marked by their index. The white color symbolizes hydrogens, the green color stands for carbon, the red color represents oxygen and blue is for nitrogen.

B. Alanine Dipeptide

Alanine dipeptide has proven itself as the most common protein to test novel algorithms, which is why we investigate it in the following. We simulate this system in vacuum, thus this protein has 66 degrees-of-freedom (22 atoms in $d = 3$ spatial dimensions) with some interaction between atoms being bonded, as drawn schematically in Fig. 5. As force-field, we make use of Amber-19ffSB, for which we have adapted the implementation from TorchMD⁶⁰ for our purposes.⁶¹ For a description on the functional form of the potential energy part of the Hamiltonian, we refer to Ref. 62. The temperature is set to $T = 300$ K and free boundary conditions are employed. For the HMC simulations, we have found that jittering with 25% can lead to non-stable simulations for larger Δt , which is why we here chose to use a jitter with 10% relative variance, i.e., $s = 0.1$. The autocorrelation times were calculated with fixed parameters after equi-

libration and obtained from timeseries with 2×10^5 MC proposals.

1. Definition and Adaptation of the Loss

We start by investigating the correlation between the loss and the autocorrelation time of the potential energy. In Fig. 6(a)-(c) we plot the loss surfaces for different choices of b in the definition of the loss of Eq. (15). A larger value of b promotes big jumps and gives less importance to small jumps, that is, big moves are more important. In all cases, we have used jittering with 10% relative variance, resulting in smooth loss surfaces. We have checked that the surface has multiple minima/maxima when we do no jittering, reiterating the importance of its inclusion. In Fig. 6(d), the corresponding autocorrelation time based on the potential energy is shown. This approach of adapting the loss function is similar in spirit to the one presented in Ref. 46, although the influence was not investigated in detail there. They chose to include a reciprocal term with a positive sign, i.e., the wanted to actively penalize small jumps in the coordinates. We have empirically checked the loss proposed in Ref. 46, but did not find suitable parameters for the free parameter λ which corresponded to a better match.

We find that using the common definition of a squared jump distance ($b = 2$) in Fig. 6(a) does not correlate well with the actual observed autocorrelation times. The region having a small loss is very large, going down to small number of integrations steps $n \approx 3$ for $\Delta t = 2.3$ fs, whereas for the autocorrelation times the region of the minimum starts around $n \approx 9$. As discussed before in Section III 2, there can be several reasons for this mismatch. On the one hand the limitation of optimizing for the lag-1 autocorrelation (made necessary to have a fast converging measure) is a potential source of mismatch and on the other hand the focus on a different observable can introduce problems. Thus, it comes as no big surprise that other definitions of the loss can provide a better correspondence. In (b) and (c) we therefore empirically test what happens to the loss surface for $b = 3$ respectively $b = 4$. We find that for $b = 3$, the minimum region of the loss shifts towards the right (larger number of integration steps n), as expected. The correspondence between the loss surface and the autocorrelation times is much better. For $b = 4$, the minimum of the loss-surface appears still to align well with the autocorrelation time, however, it appears slightly too much favored towards large n . This impression, however, changes once we consider the loss per computational cost L_n/n , which we plot in (e)-(g). Due to the small differences in amplitude between the maximal and minimal loss values when compared to the differences between autocorrelation times, the division by n massively shifts the loss towards smaller n , which is not reflected in the autocorrelation time. As for the harmonic oscillator, we also here observe a less pronounced shift towards smaller n for the autocorrelation time in

units of computational effort $n\tau$ plotted in (h). From these plots, we find the loss for $b = 4$ in (g) to provide a good correspondence, so that we will use this value for the following analysis.

2. Learning of HMC Parameters

We now turn to learning the parameters of HMC, following the general outline of the previous discussion for the harmonic oscillator. The learning rate is set to $\epsilon = 0.001$ and the other parameters of Adam⁵⁰ are kept at the default of pyTorch. We perform 10 proposals before taking one optimization step, which corresponds to training on a batch of 10 observations at each epoch. All results shown in this section are averaged over 5 independent learning trajectories for each initial $\Delta_0 t$, where each run was performed using a different random number seed responsible for the initialization of the weights C_n , the sampling of velocities, and the acceptance/reject step of HMC. In Fig. 7(a) we present again the loss surface per computational effort L_n/n for $b = 4$, where we have plotted three representative learning trajectories on for three different initial values of $\Delta_0 t$, where the color of the lines can be extracted from (b) and (c) of the same Figure. Plotted are the mean value of both Δt and n . The trajectories are obtained by initially setting $\Delta_0 t = 0.1$ fs, 0.9 fs, and 1.7 fs respectively, whereas the C_n are initialized randomly resulting in a mean value close to $N/2$. We see that all simulations approach a very similar optimum of the loss, which also corresponds to a region where the autocorrelation times are small. Note that the curves assume larger values of Δt than the region for which we had originally performed our grid-search of parameters, as is also clear from Fig. 7(b) where we show Δt as a function of learning epoch t . The values of Δt should be seen in the context of the ones used for classical MD simulations in the canonical ensemble. There, in order to capture the fastest motions and to guarantee stable simulations, one typically uses a timestep of 0.5 fs for this system (there are approaches that restrict the motion of Hydrogens, allowing via this trade-off a larger timestep). The timestep $\Delta t \approx 2.5$ we find as optimal allows for a nearly five-fold faster simulation, although of course due to the acceptance/reject step of MC some trajectories are rejected. In addition, MC guarantees the exact sampling of the true Hamiltonian since we have no effects due to the discretization of the timestep. It is interesting to note that the values of the acceptance rate around the optimal region are in the range from 50% to 60% and by this somewhat smaller than the predicted ideal value of $\approx 65\%$, although still compatible.

Fig. 7(c) shows the value of the loss L as a function of training epoch t . All simulations have similar behaving loss curve (with some differences during the initial training), which all arrive at very similar loss values. This is although the values of Δt are quite different, they cannot be distinguished by the definition of the loss. For the

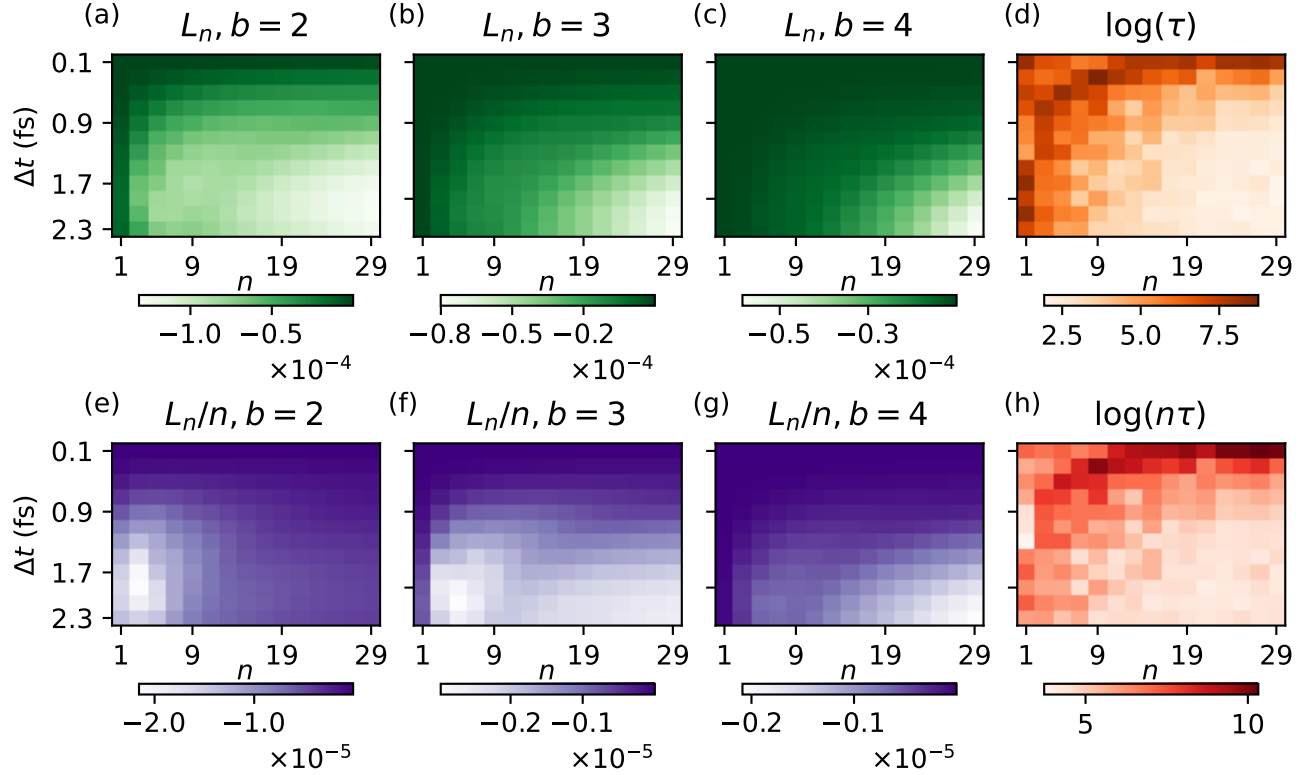


FIG. 6. Influence of the parameter b in the loss of Eq. (15) on the loss is shown for alanine dipeptide for (a) $b = 2$, (b) $b = 3$, (c) $b = 4$ on the loss surface L_n as a function of Δt and n is shown. In (e) the corresponding logarithm of the autocorrelation time of the potential energy is presented. (e)-(g) show the corresponding plots of the loss per computational effort L_n/n , and (h) shows the logarithm of the autocorrelation time in terms of computational effort $n\tau$.

start with $\Delta_0 t = 0.9$ fs, we plot also the weights given to each integration step for some selected epochs during training in Fig. 7(d). We find that starting from a random initialization giving every layer roughly the same weight, the weights move towards larger n quite fast, resulting on a large weight for our maximally considered integration step $N = 29$ for late training times t . There is some interplay between the timestep Δt and the number of integration steps n , as for a given (smaller) Δt the optimum of n does not need to coincide with the optimum for a different n and thus the optimization due to the differential set-up shifts its respective optimum. This, potentially, can influence the training, but we did not observe any obstacles in this regard.

3. Atom Dependent Timesteps

Finally, we turn towards learning not only the standard parameters of HMC, but also a version which has more parameters. We consider a timestep which is atom index dependent, i.e., we now not only have a single Δt for all atoms, but rather a different Δt_i per atom index i . As a reminder: We have 22 atoms in alanine dipeptide which means that we now have 22 different parameters

TABLE I. Autocorrelation times τ for different initial $\Delta_0 t$ for atom based timesteps and global timesteps. In the brackets we note the error of the mean.

$\Delta_0 t$	0.1 fs	0.9 fs	1.7 fs
τ for atom based Δt	12.7(2.6)	7.5(9)	7.5(1)
τ for global Δt	12.1(1.8)	10.0(1.0)	9.9(1.3)

for the timestep to optimize. For the numbering of the atoms, refer to Fig. 5. Heuristic approaches not based on gradients would most likely be much less efficient at the optimization of these many parameters, which highlights the importance of our fully differentiable approach.

Since the parameter-space is now of much higher dimension, the loss-surface cannot any longer be explored by a grid-search or even easily visualized, which is why we rely on marginalized observables only. We find that the overall optimization results in smaller loss values, as shown in Fig. 8, as is expected for a more parameterized version of the integrator. Compared to only having a single time-step Δt , we now find a loss value after training of about $L \approx -0.3 \times 10^{-5}$ (Fig. 8(a)) compared to $L \approx -0.2 \times 10^{-5}$ (Fig. 7(c)), at least for starts with $\Delta_0 t = 0.9$ fs and 1.7 fs.

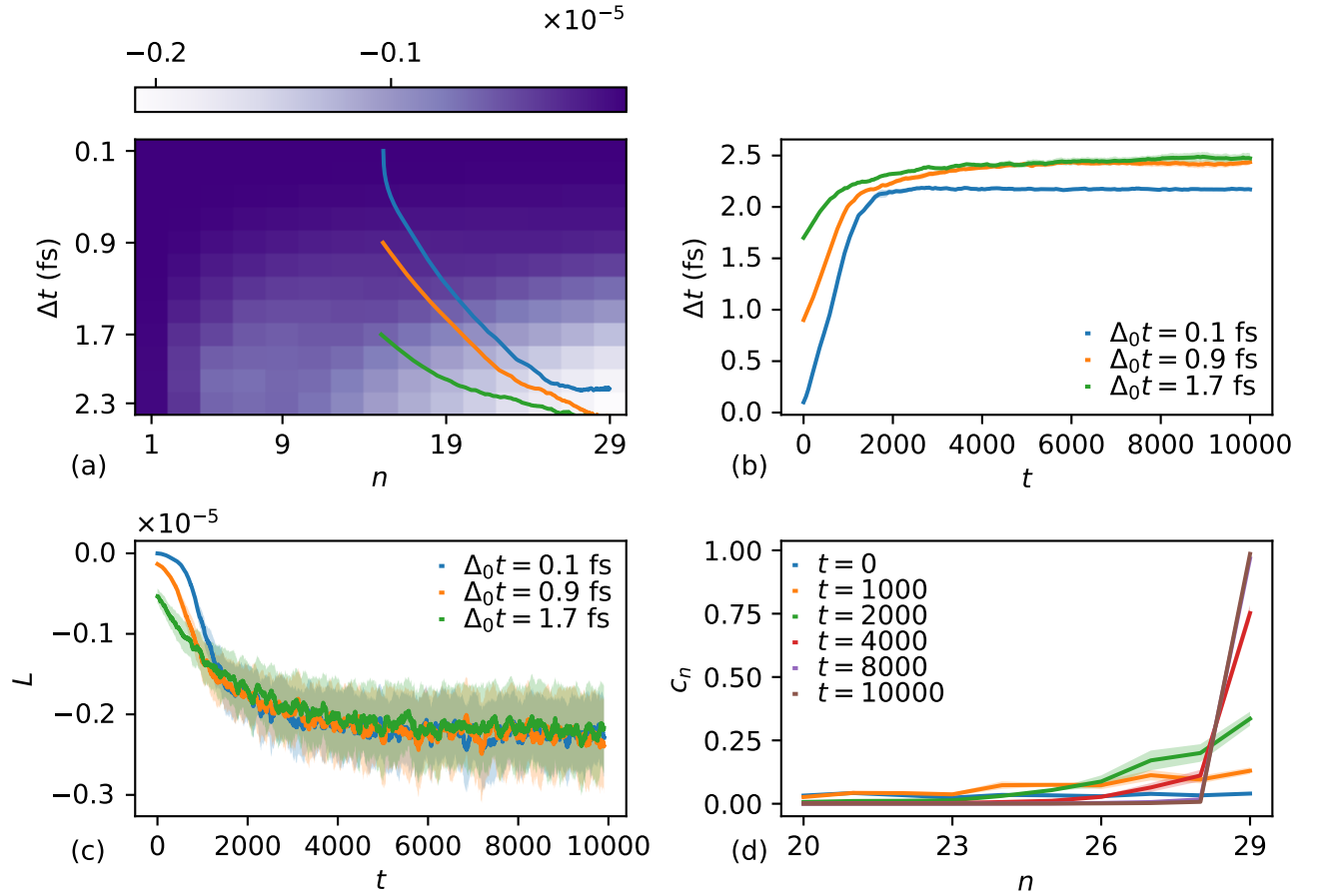


FIG. 7. (a) Loss per computational effort L_n/n as a function of Δt and n . Drawn are also three example trajectories obtained during training for initial $\Delta_0 t = 0.1$ fs, 0.7 fs, and 1.7 fs. In (b) we show the value of Δt as a function of the learning epoch t for the three initial conditions. (c) Shows the corresponding loss for these three initial conditions as a function of training epoch t . (d) displays the weights c_n as a function of the corresponding timestep n for different training epochs t as mentioned in the legend, where we have focused on the region of $n \geq 20$. In all cases (b)-(d), the shaded regions in the plot correspond to the error of the mean obtained by averaging over 5 independent runs.

In Table I we present the autocorrelation times for the potential energy. We find that using atom based Δt_i , our autocorrelation times for $\Delta_0 t = 0.9$ fs and 1.7 fs are roughly 25% lower compared to their counterpart having a global Δt . Using atom based Δt_i has only very little influence on the resulting wall-clock runtime after training, so that incorporating them in practice simply results in the reported speed-up without additional cost. For 0.1 fs, the autocorrelation times using atom based timesteps or a global timesteps are comparable, which is not surprising since for this case the loss values are also comparable.

In Fig. 8(b) we plot the atom based timesteps Δt_i as a function of epoch t for initial $\Delta_0 t = 0.9$. We find that the timestep for some atom index i is greatly improved relative to others, which corresponds to a larger timestep of these atoms. Also, the absolute value is much larger than the average value one obtains when optimizing only the “global” timestep Δt . Figure 8(c) shows the final values of Δt_i after the learning, which highlights that, at

least for the initial values of $\Delta_0 t = 0.9$ fs and 1.7 fs, one arrives at very similar behavior of Δt_i , which is an indicator that there is a local minimum of the loss for these values of Δt_i . There is up to a 3.5 fold difference between the largest and smallest timestep, highlighting the differences in the ideal parameters. For $\Delta_0 t = 0.1$ fs, many signatures as for the other two initial starting parameters remain, i.e., for many atoms the values of Δt_i follow the same trend as observed for $\Delta_0 t = 0.9$ fs and 1.7 fs, although it is unclear whether they would converge to the exactly same value in the long run using local gradient based optimizers. For all initial values of $\Delta_0 t$, we find that for the number of integration steps n we approach $n = 29$, i.e., our currently maximal allowed number of integration steps, as shown in Fig. 8(d).

To gain some physical insight into the obtained values for Δt_i , we plot in Fig. 9 the distribution of them for the different atom types of alanine dipeptide, where the values of Δt_i are obtained after training with $\Delta_0 t = 0.9$ fs. The elements are ordered after their mass, showing some

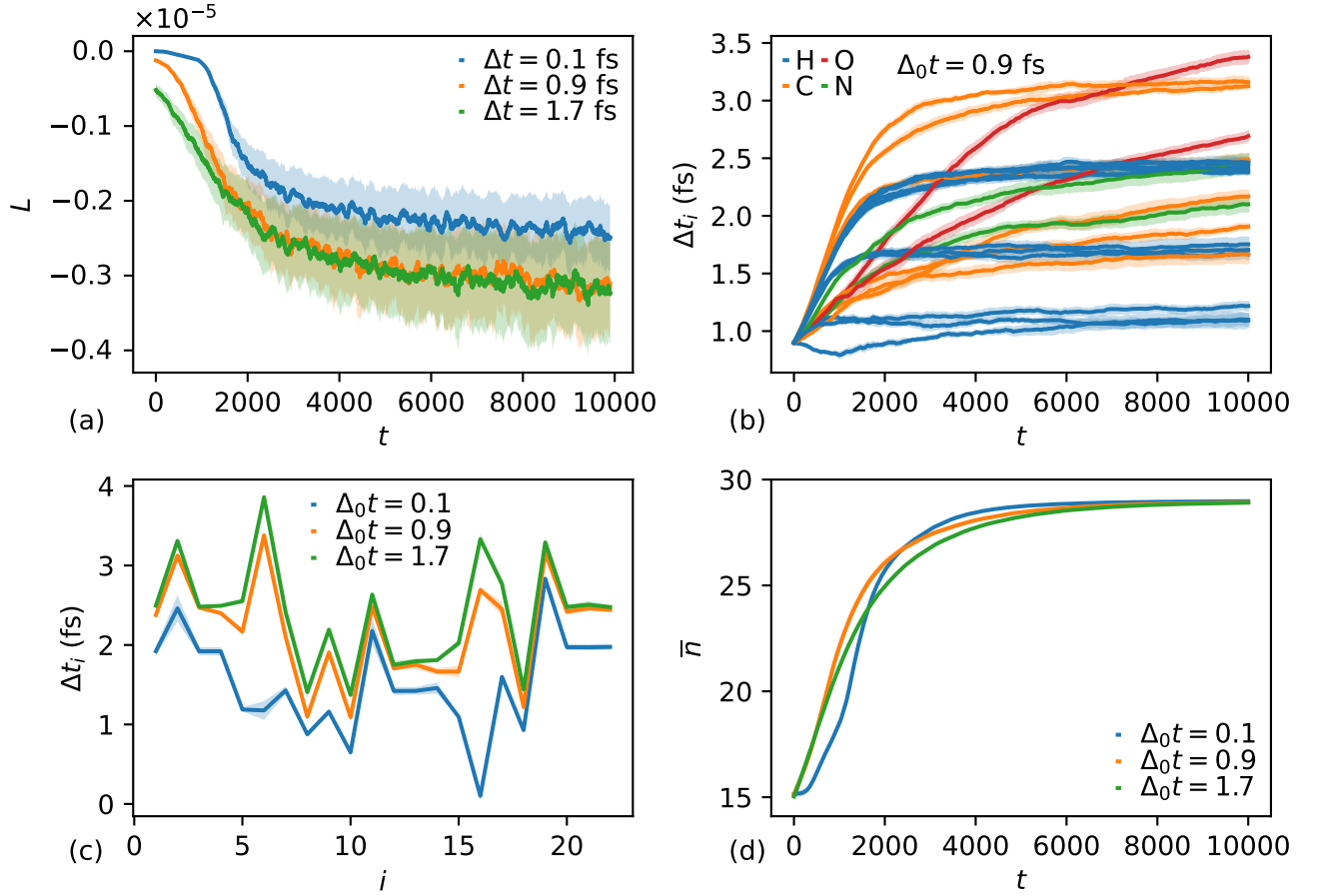


FIG. 8. (a) Loss L as a function of epoch t for different initial values of Δ_0t . (b) Shows the individual Δt_i per atom for the initial value of $\Delta t = 0.9$ fs, where we have colored atoms of the element with the same color. In (c) the final learned value of Δt_i after training is shown for the different initial values of Δt . Finally, (d) shows the mean value of integration steps \bar{n} as a function of learning epoch t .

positive correlation between the mass of the atom and the ideal timestep Δt_i . The distribution, however, is very broad in many cases. This implies that this is indeed not a simple property of atom type only, but most likely determined by its local neighborhood and the temperature. For a more detailed analysis, significantly more data for different physical systems and temperatures would be needed, which we take as an interesting endeavor.

V. CONCLUSION & OUTLOOK

We have presented a framework which allows for the gradient-based tuning of Hamiltonian Monte Carlo. Its capabilities are demonstrated for the one dimensional harmonic oscillator and alanine dipeptide simulated at constant temperature. It is found that, in both systems, our set-up allows for the optimization of the parameters of Hamiltonian Monte Carlo, leading to fast simulations and low values of the autocorrelation time.

Further, we extend the parameters of the integrator for alanine dipeptide by introducing timesteps that depend

on the atom index. We find that this can lead to lower loss values as compared to using a global timestep, which is also reflected in a lower autocorrelation time.

It would be interesting to investigate other definitions of the loss, which may provide an even stronger correlation with the autocorrelation times of the potential energy. Another direction to further speed up the simulations is the combination with hand-crafted Monte Carlo updates, which can be used in conjunction with the optimized integration to propose changes to the system. For example the pivot-move^{63,64} has been proven to be exceptionally efficient in the high-temperature phase to decorrelate samples.

While the functional form of the integrator is physically motivated and can be considered a good starting point for optimizations, the integration in general can be performed by an arbitrary function, which does not even need to be volume-preserving. In this regard, a “data-driven” integrator would be interesting, i.e., it would be interesting to investigate much more heavily parameterized versions of the integrator. Although here, in contrast to our method, the additional cost has to be con-

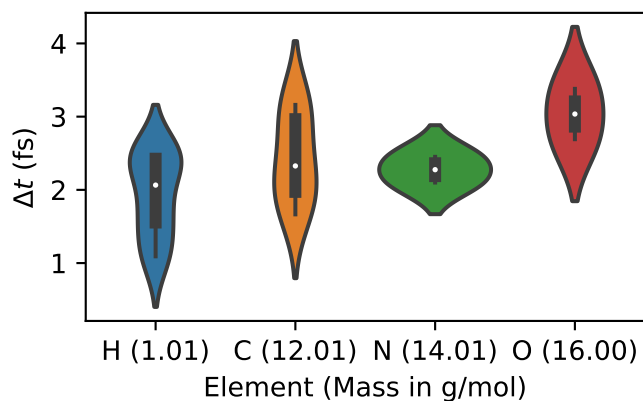


FIG. 9. Violin plot for the distribution of the timestep Δt for the four different atom types present in alanine dipeptide, taken for the start with $\Delta_0 t = 0.9$ fs. The elements are sorted according to their atom weight, which is mentioned in the brackets up to two digits.

sidered, which can eat up some advantages of a more complicated form. These integrators could then either just have (non-volume) preserving parameters which are tuned as part of the computation graph, but independent of the configuration or one can choose an architecture based on neural networks with explicit input of the systems phase-configuration⁴⁶, i.e., in some sense one would come up with a completely different functional form for the integrator. Finally, there is also potential to combine this with machine learning methods operating on graph-structured data⁶⁵, for instance with recent equivariant network architectures⁶⁶.

ACKNOWLEDGMENTS

We thank Viktor Zaverkin, Makoto Takamoto, and Mathias Niepert for useful discussion.

- ¹S. A. Hollingsworth and R. O. Dror, “Molecular dynamics simulation for all,” *Neuron* **99**, 1129–1143 (2018).
- ²A. Vitalis and R. V. Pappu, “Methods for monte carlo simulations of biomacromolecules,” *Ann. Rep. Comput. Chem.* **5**, 49–76 (2009).
- ³D. Frenkel and B. Smit, *Understanding molecular simulation: from algorithms to applications*, Vol. 1 (Elsevier, Amsterdam, 2001).
- ⁴P. H. Hünenberger, *Advances in Polymer Science*, edited by C. Holm and K. Kremer, Vol. 174 (Springer, Berlin, Heidelberg, 2005) Chap. Thermostat algorithms for molecular dynamics simulations, pp. 105–149.
- ⁵M. P. Allen and D. J. Tildesley, *Computer simulation of liquids* (Oxford University Press, Oxford, 2017).
- ⁶R. M. Neal, *Handbook of Markov Chain Monte Carlo*, edited by S. Brooks, A. Gelman, G. Jones, and X.-L. Meng, 11 (Chapman and Hall/CRC, New York, 2011) Chap. MCMC using Hamiltonian dynamics, p. 2.
- ⁷R. M. Neal, *Bayesian learning for neural networks*, Lecture Notes in Statistics, Vol. 118 (Springer, New York, 2012).
- ⁸M. Betancourt, “A conceptual introduction to Hamiltonian Monte Carlo,” arXiv:1701.02434 (2017).

- ⁹S. Duane, A. D. Kennedy, B. J. Pendleton, and D. Roweth, “Hybrid Monte Carlo,” *Phys. Lett. B* **195**, 216–222 (1987).
- ¹⁰F. Rosenblatt, “Principles of neurodynamics. perceptrons and the theory of brain mechanisms,” Tech. Rep. (Cornell Aeronautical Lab, Buffalo, 1961).
- ¹¹D. E. Rumelhart and J. L. McClelland, “Learning internal representations by error propagation,” in *Parallel Distributed Processing: Explorations in the Microstructure of Cognition: Foundations* (MIT Press, Cambridge, 1987) pp. 318–362.
- ¹²J. Hermans, “The amino acid dipeptide: Small but still influential after 50 years,” *Proc. Nat. Acad. Sci.* **108**, 3095–3096 (2011).
- ¹³M. E. Newman and G. T. Barkema, *Monte Carlo methods in statistical physics* (Clarendon Press, 1999).
- ¹⁴W. Janke, “Monte Carlo simulations in statistical physics: From basic principles to advanced applications,” in *Order, Disorder and Criticality*, Advanced Problems of Phase Transition Theory, Vol. 3, edited by Y. Holovatch (World Scientific, Singapore, 2013) pp. 93–166.
- ¹⁵N. Metropolis, A. W. Rosenbluth, M. N. Rosenbluth, A. H. Teller, and E. Teller, “Equation of state calculations by fast computing machines,” *J. Chem. Phys.* **21**, 1087–1092 (1953).
- ¹⁶W. K. Hastings, “Monte Carlo sampling methods using Markov chains and their applications,” *Biometrika* **57**, 97–109 (1970).
- ¹⁷J. Deutsch, “Long range moves for high density polymer simulations,” *J. Chem. Phys.* **108**, 8849–8854 (1997).
- ¹⁸H. Christiansen, S. Majumder, and W. Janke, “Phase ordering kinetics of the long-range Ising model,” *Phys. Rev. E* **99**, 011301 (2019).
- ¹⁹H. Christiansen, S. Majumder, M. Henkel, and W. Janke, “Aging in the long-range Ising model,” *Phys. Rev. Lett.* **125**, 180601 (2020).
- ²⁰T. W. Kibble, “Some implications of a cosmological phase transition,” *Phys. Rep.* **67**, 183–199 (1980).
- ²¹W. H. Zurek, “Cosmological experiments in condensed matter systems,” *Phys. Rep.* **276**, 177–221 (1996).
- ²²W. C. Swope, H. C. Andersen, P. H. Berens, and K. R. Wilson, “A computer simulation method for the calculation of equilibrium constants for the formation of physical clusters of molecules: Application to small water clusters,” *J. Chem. Phys.* **76**, 637–649 (1982).
- ²³S. Prokhorenko, K. Kalke, Y. Nahas, and L. Bellaiche, “Large scale hybrid Monte Carlo simulations for structure and property prediction,” *npj Comput. Mat.* **4**, 80 (2018).
- ²⁴J. Hu, A. Ma, and A. R. Dinner, “Monte Carlo simulations of biomolecules: The MC module in CHARMM,” *J. Comput. Chem.* **27**, 203–216 (2006).
- ²⁵M. Fernández-Pendás, B. Escibano, T. Radivojević, and E. Akhmatskaya, “Constant pressure hybrid Monte Carlo simulations in GROMACS,” *J. Mol. Model.* **20**, 1–10 (2014).
- ²⁶J. Chodera, A. Rizzi, L. Naden, K. Beauchamp, P. Grinaway, J. Fass, A. Wade, B. Rustenburg, I. Pulido, G. A. Ross, M. Henry, A. Krämer, H. B. Macdonald, J. Rodríguez-Guerra, I. Zhang, A. Simmonett, D. W. Swenson, M. J. Williamson, J. Fennick, S. Roet, S. Boothroyd, A. Silveira, and D. Ruffa, “choderalab/openmmtools: 0.21.5,” (2022).
- ²⁷S. Toxvaerd, O. J. Heilmann, and J. C. Dyre, “Energy conservation in molecular dynamics simulations of classical systems,” *J. Chem. Phys.* **136** (2012).
- ²⁸J. Song, S. Zhao, and S. Ermon, “A-nice-mc: Adversarial training for MCMC,” *Adv. Neur. Inf. Proc. Sys.* **30** (2017).
- ²⁹S. Liu and S. Sun, “Adversarially training MCMC with non-volume-preserving flows,” *Entropy* **24**, 415 (2022).
- ³⁰A. Beskos, N. Pillai, G. Roberts, J.-M. Sanz-Serna, and A. Stuart, “Optimal tuning of the hybrid Monte Carlo algorithm,” *Bernoulli* **19**, 1501–1534 (2013).
- ³¹Z. Wang, S. Mohamed, and N. Freitas, “Adaptive Hamiltonian and Riemann manifold Monte Carlo,” *Int. Conf. Mach. Learn.* **1462–1470** (2013).
- ³²M. D. Hoffman and A. Gelman, “The No-U-Turn sampler: adaptively setting path lengths in Hamiltonian Monte Carlo,” *J.*

- Mach. Learn. Res. **15**, 1593–1623 (2014).
- ³³M. Hoffman, A. Radul, and P. Sountsov, “An adaptive-MCMC scheme for setting trajectory lengths in Hamiltonian Monte Carlo,” *Int. Conf. Artificial Intel. Stat.*, 3907–3915 (2021).
 - ³⁴M. Girolami and B. Calderhead, “Riemann manifold Langevin and Hamiltonian Monte Carlo methods,” *J. Royal Stat. Soc. Ser. B: Stati. Method.* **73**, 123–214 (2011).
 - ³⁵M. D. Parno and Y. M. Marzouk, “Transport map accelerated markov chain monte carlo,” *J. Uncert. Quant.* **6**, 645–682 (2018).
 - ³⁶M. Betancourt, “Incomplete reparameterizations and equivalent metrics,” *arXiv:1910.09407* (2019).
 - ³⁷M. Hoffman, P. Sountsov, J. V. Dillon, I. Langmore, D. Tran, and S. Vasudevan, “Neutra-lizing bad geometry in hamiltonian monte carlo using neural transport,” *arXiv:1903.03704* (2019).
 - ³⁸L. Grenioux, A. Durmus, É. Moulines, and M. Gabrié, “On sampling with approximate transport maps,” *arXiv:2302.04763* (2023).
 - ³⁹J. A. Brofos and R. R. Lederman, “On numerical considerations for riemannian manifold hamiltonian monte carlo,” *arXiv:2111.09995* (2021).
 - ⁴⁰T. A. Bojesen, “Policy-guided Monte Carlo: Reinforcement-learning Markov Chain dynamics,” *Phys. Rev. E* **98**, 063303 (2018).
 - ⁴¹E. G. Tabak and E. Vanden-Eijnden, “Density estimation by dual ascent of the log-likelihood,” *Comm. Math. Sci.* **8**, 217–233 (2010).
 - ⁴²E. G. Tabak and C. V. Turner, “A family of nonparametric density estimation algorithms,” *Comm. Pure Appl. Math.* **66**, 145–164 (2013).
 - ⁴³G. Papamakarios, E. Nalisnick, D. J. Rezende, S. Mohamed, and B. Lakshminarayanan, “Normalizing flows for probabilistic modeling and inference,” *J. Mach. Learn. Res.* **22**, 2617–2680 (2021).
 - ⁴⁴F. Noé, S. Olsson, J. Köhler, and H. Wu, “Boltzmann generators: Sampling equilibrium states of many-body systems with deep learning,” *Science* **365**, eaaw1147 (2019).
 - ⁴⁵M. Gabrié, G. M. Rotskoff, and E. Vanden-Eijnden, “Adaptive Monte Carlo augmented with normalizing flows,” *Proc. Nat. Acad. Sci.* **119**, e2109420119 (2022).
 - ⁴⁶D. Levy, M. D. Hoffman, and J. Sohl-Dickstein, “Generalizing Hamiltonian Monte Carlo with neural networks,” *Int. Conf. Learn. Repr.* (2018).
 - ⁴⁷A. Paszke, S. Gross, F. Massa, A. Lerer, J. Bradbury, G. Chanan, T. Killeen, Z. Lin, N. Gimelshein, L. Antiga, A. Desmaison, A. Kopf, E. Yang, Z. DeVito, M. Raison, A. Tejani, S. Chilamkurthy, B. Steiner, L. Fang, J. Bai, and S. Chintala, “PyTorch: An imperative style, high-performance deep learning library,” *Adv. Neur. Inf. Proc. Systems*, 8024–8035 (2019).
 - ⁴⁸L. B. Rall, *Automatic differentiation: Techniques and applications*, Lecture Notes in Computer Science (Springer, Berlin, Heidelberg, 1981).
 - ⁴⁹A. Paszke, S. Gross, S. Chintala, G. Chanan, E. Yang, Z. DeVito, Z. Lin, A. Desmaison, L. Antiga, and A. Lerer, “Automatic differentiation in pyTorch,” *Adv. Neur. Inf. Proc. Sys.* (2017).
 - ⁵⁰D. P. Kingma and J. Ba, “Adam: A method for stochastic optimization,” *Int. Conf. Learn. Repr.* (2014).
 - ⁵¹J. V. Dillon, I. Langmore, D. Tran, E. Brevdo, S. Vasudevan, D. Moore, B. Patton, A. Alemi, M. Hoffman, and R. A. Saurous, “Tensorflow distributions,” *arXiv:1711.10604* (2017).
 - ⁵²C. J. Geyer, “Practical Markov chain Monte Carlo,” *Stat. Sci.*, 473–483 (1992).
 - ⁵³A. Beskos, G. Roberts, and A. Stuart, “Optimal scalings for local Metropolis–Hastings chains on nonproduct targets in high dimensions,” *Ann. Appl. Probab.* **19**, 863–898 (2009).
 - ⁵⁴C. Pasarica and A. Gelman, “Adaptively scaling the Metropolis algorithm using expected squared jumped distance,” *Stat. Sinica*, 343–364 (2010).
 - ⁵⁵P. Sountsov and M. D. Hoffman, “Focusing on difficult directions for learning HMC trajectory lengths,” *arXiv:2110.11576* (2021).
 - ⁵⁶A. Vaswani, N. Shazeer, N. Parmar, J. Uszkoreit, L. Jones, A. N. Gomez, Ł. Kaiser, and I. Polosukhin, “Attention is all you need,” *Adv. Neur. Inf. Proc. Sys.* **30** (2017).
 - ⁵⁷R. D. Engle, R. D. Skeel, and M. Drees, “Monitoring energy drift with shadow Hamiltonians,” *J. Comput. Phys.* **206**, 432–452 (2005).
 - ⁵⁸O. A. Zolotov and V. E. Zalizniak, “Accurate energy conservation in molecular dynamics simulation,” *Nanosyst. Phys. Chem. Math.* **4**, 657–669 (2013).
 - ⁵⁹S. Kim, “Time step and shadow Hamiltonian in molecular dynamics simulations,” *J. Korean Phys. Soc.* **67**, 418–422 (2015).
 - ⁶⁰S. Doerr, M. Majewski, A. Pérez, A. Kramer, C. Clementi, F. Noe, T. Giorgino, and G. De Fabritiis, “Torchmd: A deep learning framework for molecular simulations,” *J. Chem. Theo. Comput.* **17**, 2355–2363 (2021).
 - ⁶¹In the original implementation, the gradients calculated by automatic differentiation needed to make this problem fully-differentiable are not preserved. We have adapted the code to preserve those.
 - ⁶²C. Tian, K. Kasavajhala, K. A. Belfon, L. Raguette, H. Huang, A. N. Miguez, J. Bickel, Y. Wang, J. Pincay, Q. Wu, *et al.*, “ff19sb: Amino-acid-specific protein backbone parameters trained against quantum mechanics energy surfaces in solution,” *J. Chem. Theo. Comput.* **16**, 528–552 (2019).
 - ⁶³M. Lal and D. Spencer, “Monte Carlo computer simulation of chain molecules: V. Flexibility of n-alkane molecules,” *Mol. Phys.* **26**, 1–6 (1973).
 - ⁶⁴N. Madras and A. D. Sokal, “The pivot algorithm: a highly efficient Monte Carlo method for the self-avoiding walk,” *J. Stat. Phys.* **50**, 109–186 (1988).
 - ⁶⁵D. Bacciu, F. Errica, A. Micheli, and M. Podda, “A gentle introduction to deep learning for graphs,” *Neur. Net.* **129**, 203–221 (2020).
 - ⁶⁶M. M. Bronstein, J. Bruna, T. Cohen, and P. Veličković, “Geometric deep learning: Grids, groups, graphs, geodesics, and gauges,” *arXiv:2104.13478* (2021).